Assessing decadal to centennial scale nonstationary variability in meteorological drought trends

Kyungmin Sung[1], Max Torbenson[2], James H. Stagge[1],

[1]Civil, Environmental and Geodetics Engineering, The Ohio State University, Columbus, Ohio
[2]Department of Geography, Johannes Gutenberg Universität, Mainz, Germany

Correspondence to: Kyungmin Sung (sung.229@osu.edu)

Abstract. There are indications that the reference climatology underlying meteorological drought has shown non-stationarity at seasonal, decadal, and centennial time scales, impacting the interpretation of normalized drought indices and potentially producing serious ecological, economic, and social consequences. Analyzing these trends in the meteorological drought climatology beyond the 100-year observation period contributes to a better understanding of the non-stationary changes, ultimately determining whether they are within the range of natural variability or outside this range. To accomplish this, our study introduces a novel approach to incorporate unevenly scaled tree-ring proxy data (NASPA) with instrumental precipitation datasets by first temporal downscaling the proxy data to produce a regular time series, and then modeling climate non-stationarity while simultaneously correcting model induced bias. This new modeling approach was applied to 14 sites across the continental United States using the 3-month Standardized Precipitation Index (SPI) as a basis. Findings showed locations which have experienced recent rapid shifts towards drier or wetter conditions during the instrumental period compared to the past 1000 years, with drying trends generally in the west and wetting trends in the east. This study also found that seasonal shifts have occurred in some regions recently, with seasonality changes most notable for southern gauges. We expect that our new approach provides a foundation for incorporating various datasets to examine non-stationary variability in long-term precipitation climatology and to confirm the spatial patterns noted here in greater detail.

1 Introduction

Understanding meteorological drought trends is important as the entangled impacts of anthropogenic climate change and natural climate variability have complicated patterns of precipitation change over the last century (Ault, 2020; Schubert et al., 2016). Drought severity and duration has changed over time at seasonal, interannual or centennial scales, with subsequent impacts on human and ecological systems (Trenberth, 2011; Van Loon et al., 2016). Many studies have investigated trends or shifts in drought related to climate change (Marvel et al., 2021; Williams et al., 2020; Mishra et al., 2010; Marvel et al., 2019; Trenberth et al., 2014). Previous research has relied heavily on observed or remotely sensed precipitation records, which often do not exceed 100 years. Although such observations can capture modern drought trends,

100 years of data are not sufficient for determining whether recent drought trends are a part of long-term cyclic variability, due to recent unprecedented trends, or a combination of the two (Easterling et al., 2000; Cook et al., 2015).

In addition, previous studies have indicated that precipitation seasonality has changed during the observed period: those changes include increases in the amplitude between the wet and dry seasons, or temporal shifts in the driest/wettest period (Marvel et al., 2021; Weiss et al., 2009; Pal et al., 2013). Even without substantial changes in the annual mean precipitation, shifts in precipitation seasonality can have significant impact on local ecosystems or man-made water management schemes like reservoirs that rely on storing and releasing seasonal flow. As a result, understanding seasonal cycles and non-stationary shifts in seasonality are important for building adaptive and robust water management schemes (Konapala et al., 2020). For climate projections of the next 100 years, Marvel et al. (2021) found projected changes in annual precipitation cycles across the U.S. Midwest and Upper Great Plains. This region is projected to undergo a shift in peak precipitation to earlier in the year without substantial changes in precipitation. This study also projected an increase in precipitation during the wettest season (winter) in the Northwest and Southeast US, thereby increasing the seasonal variance in precipitation. Changes in seasonality or seasonal variance can be better understood when viewed in historical context using a much longer time window to determine whether they are within the range of natural climate variability or outside this range (Coats et al., 2015).

Therefore, much longer time scales are needed for a comprehensive understanding of non-stationary drought trends, preferably using a multi-centennial time scale (Torbenson and Stahle, 2018; Herweijer et al., 2007; Cook et al., 2010a; Diffenbaugh et al., 2015). Paleoclimate reconstructions use environmental proxies, such as tree-ring chronologies or speleothem records that physically record some aspect of climate, and can cover a much longer period than the instrumental observations (Cook et al., 2016). For example, this study uses a reconstruction of precipitation across North America based on tree-rings, from which the relative availability of regional precipitation or soil moisture can be inferred based on increased or decreased annual growth. This particular reconstruction is a gridded continental-scale reconstruction, rather than a regional or local reconstruction. Large-scale gridded reconstructions sacrifice some local precision, but have the benefit of generating a single, complete dataset based on a common methodology, which can leverage a larger catalog of chronologies. Several such gridded hydrometeorological reconstruction datasets using tree-ring proxies are available across North America. The North American Drought Atlas (NADA; Cook et al., 1999) reconstructs Palmer Drought Severity Index (PDSI; Palmer, 1965) in June to August (JJA) from 0-2006 A.D. and has been used to determine historic drought severities (Cook et al., 2010b; Cook and Krusic, 2008). The North American Seasonal Precipitation Atlas (NASPA) is another precipitation reconstruction recently developed with two distinct seasons: December to April (DJFMA) and May to July (MJJ) (Stahle et al., 2020). The NASPA dataset provides both SPI and averaged precipitation for both the cool and warm seasons. The NASPA is used here since it covers the past 2,000 years and contains cool and warm season records for each year. Over 2,000 years of sub-annual scale records enable an investigation of non-stationary drought trends and seasonal shifts across multi-centennial scale if they can be combined with recent observed instrumental datasets (Trenberth et al., 2014; Marvel et al., 2019; Cook et al., 2016).

Despite the value of long reconstructions, comparing meteorological drought trends across observed and proxy-based reconstruction datasets is challenging as these data types are often not directly compatible (Baek et al., 2017; St. George et al., 2010). The first challenge is that each dataset often has non-negligible biases. Biases in proxy reconstructions can be caused by indirect measurement of the target variable, e.g., precipitation, by way of tree-ring growth. For example, bias can be introduced during the standardization process, designed to isolate the interannual signal from the long-term geometric growth of a tree. Trees also have physiological responses to continuous extreme drought or pluvials, which can limit variance at the extremes (Franke et al., 2013; Robeson et al., 2020). Even among gridded datasets based on gauge observations, bias can be introduced by the use of imperfect transforming algorithms (Sun et al., 2018), due to orographic induced bias, underestimation of trace precipitation amounts (Goodison et al. 1998), or wind-related undercatch (Pollock et al., 2018). Thereby, precipitation measurements for the same period can differ across datasets. These biases can cause one dataset to systematically under- or overestimate precipitation compared to other datasets (Robeson et al., 2020), or to modify the range of estimates. Quantifying and minimizing those biases is necessary to merge disparate datasets and analyze a common trend across various datasets.

A second challenge for merging reconstructions and observations is their heterogeneous spatial and temporal scales (Cook and Krusic, 2008). For example, the NASPA reconstructions are made up of two values per year, but the seasonal windows of the time series are of different length and do not span the entire year (Fig. 1). Instrumental datasets can have sub-daily, daily, or monthly temporal scales (Howard et al., 2021). Therefore, time scale must be unified if one is to merge instrumental and reconstructed datasets to observe common non-stationary seasonal trends. In addition, the spatial resolution of gridded datasets varies, and centers of those grid cells are not always matched. Thus, matching co-located grid cells through creating a common spatial resolution is an important aspect in representing common characteristics in precipitation (Abatzoglou, 2013).

This study is designed to address the challenge of merging precipitation datasets with varied biases and temporal scales to calculate a common Standardized Precipitation Index (SPI; Guttman, 1999) meteorological drought series that incorporates non-stationarity. The objectives of this study are therefore to (1) downscale the NASPA time series into monthly timescale, (2) identify unique biases inherent in different precipitation data and remove those biases, and (3) analyze non-stationary long-term trends varying by season.

Here, we downscale NASPA data to a monthly scale using K-nearest neighbors (KNN). KNN is a statistical downscaling technique widely used in hydrologic time series (Raje and Mujumdar, 2011; Gangopadhyay et al., 2005; Gutmann et al., 2012) such as reconstructing annual streamflow from tree-ring chronology data or producing local-scale precipitation or temperature time series using neighboring climate stations (Gangopadhyay et al., 2005, 2009). Our study adopts this method to temporally downscale NASPA data from bi-annual to a monthly scale. Second, we develop a model to simultaneously analyze unique biases in proxy and instrumental datasets, account for them, and then analyze a non-linear trend common across the datasets. Ultimately, our approach allows us to simultaneously model long-term trends in different seasons.

2 Methodology

This study seeks to merge 3-month precipitation data from two datasets derived from observations (GridMET and CRU) with the North American Seasonal Precipitation Atlas (NASPA) reconstructions by accounting for underlying biases before

100   identifying a common long-term signal. The overall approach is to first temporally downscale reconstructed NASPA precipitation data into a monthly resolution. A hierarchical GAM model is then developed and applied to merge the datasets. This approach is tested at 14 sites across the continental US. Section 2.1 presents precipitation datasets used in this study, while Section 2.2 provides background on SPI calculation. Section 2.3 introduces the novel approach for temporal downscaling of the reconstructed precipitation and Section 2.4 describes the GAM model for merging disparate datasets and

105   analyzing meteorological drought trends using the SPI framework.

2.1. Data

An additional precipitation dataset, from the Global Precipitation Climatology Center (GPCC; Becker et al., 2013), was used to temporally downscale/disaggregate the NASPA into monthly values as this was the instrumental target for the NASPA reconstructions. The underlying precipitation datasets used in the analyses presented here are as follows:

110   NASPA: The North American Seasonal Precipitation Atlas is a dataset of gridded reconstructions of precipitation, based on a network of 986 tree-ring chronologies from across the North American continent (Stahle et al., 2020). Precipitation totals and SPI are reconstructed for December–April (DJFMA) and May-July (MJJ) across a 0.5° x 0.5° grid, resulting in a total of 6812 grid cells (Stahle et al., 2020). The length of the reconstructions varies across space and between seasons but have a maximum of over 2,000 years at many locations, particularly in the western US.

115   The NASPA reconstructions target Global Precipitation Climatology Center data (GPCC), applied at each GPCC grid point using 16 ensembles of tree-ring chronology-based regressions of differing weights (Stahle et al., 2020). An additional NASPA reconstruction dataset for MJJ exists for the period 1400-2016, in which shared variance between DJFMA and MJJ precipitation estimates are removed from the following MJJ reconstruction (Torbenson et al., 2021). Our model uses the DJFMA and original, non-processed MJJ reconstructions from the 16-ensemble mean as to maximize the period of study and

120   because the GAM model accounts for some level of persistence.

CRU TS: Climate Research Unit TS4.01 (CRU) is a 0.5° x 0.5° gridded dataset of monthly climate. It is based on individual station observations which are directly interpolated to a gridded scale (New et al., 2000; Harris et al., 2020). This study used version 4.01 which covers the period 1901-2018 (Harris et al., 2020).

GridMET: The Gridded Observed Meteorological data (GridMET) is a gridded (1/24° x 1/24°) dataset of daily resolution

125   available from 1950–2020, for the US (Maurer et al., 2002). GridMET is constructed by combining direct daily gauge observations with regional scale reanalysis to fill gaps (Abatzoglou, 2013). The highly accurate and well-distributed precipitation data is used as the base observations to calibrate CRU and NASPA datasets.

GPCC v7: The Global Precipitation Climatology Project (GPCC) is a gridded precipitation product built on gauge-based precipitation. The monthly-resolved GPCC v7 covers the period 1901 to 2013 at a 0.5° x 0.5° spatial resolution (Becker et al., 2013). Since the NASPA reconstructions were originally calibrated based on GPCC data, we assumed that precipitation time series of GPCC and NASPA share the same probability distribution function at the same grid cell. Thus, this study uses monthly GPCC data to best mimic the intra-annual characteristics for temporally downscaling and disaggregating NASPA estimates to monthly time series. GPCC is only used for temporal disaggregation of NASPA data and is not included in the hierarchical GAM model.

2.2 Drought Measurement

Drought is defined as a lack of water within the hydrologic cycle relative to the given climatology of a location. Meteorological drought refers to a deficit of precipitation relative to typical conditions for a location and period. The severity of meteorological drought is often measured by the Standard Precipitation Index (SPI). The SPI is calculated by fitting n-days accumulated precipitation time series to a set of probability distributions for each period's climatology and then using these distributions to convert accumulated precipitation into the standard normal distribution (Lloyd-Hughes and Saunders, 2002; Stagge et al., 2017, 2015; Guttman, 1999). SPI values therefore represent the number of standard deviations from typical conditions for a site and time of the year. The SPI is widely used for studying or monitoring meteorological drought, particularly by the U.S Drought Monitor and World Meteorological Organization (WMO). It has unique strengths of using precipitation only: a simple data requirement and calculation process, and straightforward interpretation between averaged precipitation and drought severity (Dai, 2011; Ukkola et al., 2020; Svoboda et al., 2002).

In this study, we use a 3-month moving average of precipitation (SPI-3) to provide seasonal characteristics of drought (Patel et al., 2007). We present SPI-3 values of -1.5, 0, and 1.5, which are equivalent to the 6th percentile, mean, and 94th percentile thresholds of a fitted two-parameter Gamma distribution. These thresholds represent the precipitation associated with severe dry, typical, and wet conditions for each location.

2.3 Temporal downscaling using K nearest neighbor resampling

K-nearest neighbor (KNN) is a downscaling technique designed to estimate some target information by searching a set of historical catalogs of the target vector and finding the k most similar analogs, where k can be any number of the user's choice (Gangopadhyay et al., 2005). In this study, monthly GPCC time series were used as sampling catalogs for selecting target vectors (annual precipitation sequences) based on NASPA values. More specifically, the goal is to insert K historical 13-month precipitation sequences from the GPCC library into a given year of the NASPA reconstruction based on similarity to the recorded SPI values during the prior and current year. Because this is a resampling approach, multiple (k = 10) annual historical sequences are inserted for each year of the reconstruction to simulate uncertainty.
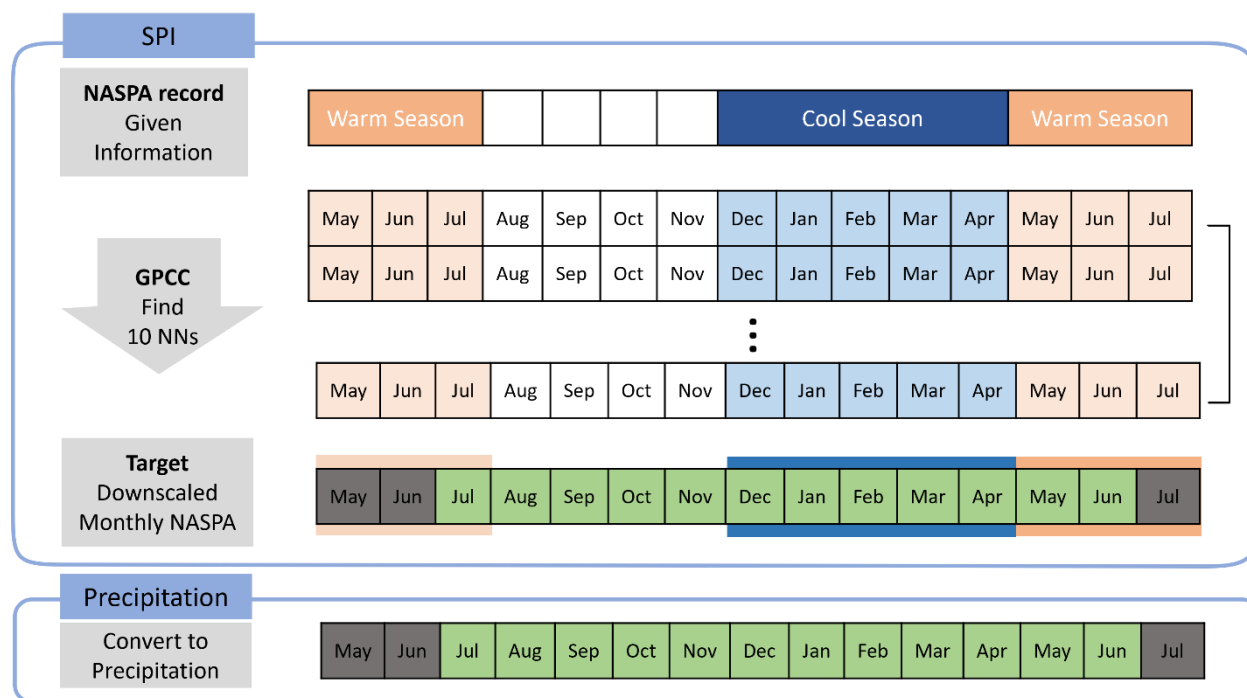
Figure 1. Framework for the temporal downscaling process. Monthly scale NASPA (3-months averaged precipitation) time series is constructed using this process. This method is applied for every year of reconstruction.

Figure 1 outlines the temporal downscaling process using KNN. For each year, NASPA values were constructed as the target vector using three data points: SPI-3 during the previous year's MJJ period, SPI-5 in this year's DJFMA period, and SPI-3 in this year's MJJ period. SPI-3 and SPI-5 values calculated from the GPCC instrumental period (1901-2013) for the same location were constructed as the data library. GPCC was used because it formed the basis for the original NASPA reconstruction (Stahle et al., 2020). Second, for each year, we calculated the Euclidean distances between the target vector from NASPA and the available GPCC library to select 10 sequences (k=10) from the GPCC SPI time series which have the closest Euclidean distance to the target NASPA SPI values. Note that resampled sequences are permitted to be any historical 13-months SPI series, regardless of whether the months align, increasing the number of available sequences from 113 (years in the GPCC dataset) to 1356 (years × months). This is possible because SPI is agnostic to season, each month follows a standard normal distribution. Then, the ten monthly resampled SPI-3 time series were averaged and inserted into the targeted year of the NASPA. Lastly, the substituted SPI-3 time series were converted back to the 3-months averaged precipitation using the 2-parameter Gamma distributions from each month of GPCC dataset.

Overall, our downscaling approach provides a few advantages: first, it reflects the compatibility of the climate field as it searches analogs from the same location. Second, direct resampling based on similarity from the GPCC sample field incorporates realistic seasonal progression and persistence of the SPI. Third, the K neighbors creates an ensemble of time series, incorporating uncertainty (Gangopadhyay et al., 2005).

Downscaling skill was measured by normalized mean absolute error (nMAE) using the following equations:

$$nMAE = \frac{\sum_{Month,year} |GPCC - NASPA|}{\sum_{Month,year} GPCC} \tag{1}$$

180 where GPCC represents the observed precipitation during the instrumental period and NASPA represents the ensemble mean
of the reconstructed precipitation after applying the KNN downscaling to the NASPA reconstruction.

2.4 Bias correction using Hierarchical GAM

Generalized additive models (GAM) are statistical models that permit regression using non-linear smooth functions instead
of, or in addition to, linear covariates. GAMS are a subset of Generalized Linear Models (GLM), meaning their regression
185 terms can represent parameters for data with distributions other than Normal. However, where most GLMs apply linear
regression principles to model a distribution's parameters, GAMs can include non-linear terms (Simpson, 2018; Wood,
2008; Pedersen et al., 2019). When non-linear terms are applied to time series data, GAMs also permit spanning irregularly
sampled data to model complex and non-linear drought trends.

GAM models have been previously applied to accumulated precipitation data to estimate the parameters of the 2-parameter
190 gamma distribution SPI under non-stationary climate conditions (Stagge and Sung, 2022; Shiau, 2020; Sung and Stagge,
2022). This study relies on the non-stationary SPI approach introduced in Stagge and Sung (2022) and applied in Sung and
Stagge (2022). In this approach, the two parameters (mean and shape) are modeled as a function of two covariates of time:
year and month. Here, we expand this approach, by adding a hierarchical grouping variable to simultaneously model
common seasonal-specific long-term trends across datasets, while also incorporating variability at the group level following
195 the approach of Pederson et al. (2019). When applied to our model, this involves a smoothed long-term trend that is common
to all datasets (CRU, GridMET, and NASPA) and differences for the seasonal terms that repeat annually at the group-level
(climate dataset) (Pedersen et al., 2019). This model estimates the mean and shape parameters of 2-parameter Gamma
distribution. The detailed model framework is shown below in Equations 1 and 2.

$$P_{3month} = gamma(\mu, \alpha)$$

$$\mu = \beta_{0,model} + \beta_{s1}f(X_{month}, \text{by=model}) + \beta_{s2}f(X_{year}, X_{month}) \tag{1}$$

$$\frac{1}{\log(\alpha)} = \beta_{0,model} + \beta_{s1}f(X_{month}, \text{by=model}) + \beta_{s2}f(X_{year}, X_{month}) \tag{2}$$

where P_{3month} represents the 3-month moving average precipitation, μ represents the mean, and α represents the shape
200 parameter of the gamma distribution. The gamma distribution scale parameter is calculated as β=μ/α where β represents the
scale parameter. The underlying principle of the model is that there exists a single best estimate of the precipitation
distribution at any given time, described by the mean and shape parameters of the gamma distribution that changes
seasonally and can also change slowly on a multi-decadal scale, $f(X_{year}, X_{month})$. Similar to quantile mapping bias correction
(Lanzante et al., 2018; Ho et al., 2012), the $B_{0, model}+B_1 f(X_{month}, model)$ terms allow for adjustments in mean and shape based

205 on the month and the model. The model is therefore capable of modeling trends and correcting data-induced bias simultaneously.

As previously described, this model has a single common smoother, $f(X_{year}, X_{month})$, which is shared across all datasets. For the common smooth term, $f(X_{year}, X_{month})$, we applied a tensor product which allows the parameter to vary smoothly in two-dimensions, seasonally and inter-annually. Deriving β_{s2} in terms of year and months allows for non-linear annual trends for

210 each month while constraining these trends to be smooth through time. As such, the tensor product can simultaneously model typical wet or dry seasonality, shifts of those periods to earlier or later in the year, and non-stationary changes in the long-term. The tensor spline approach to model trends in two time dimensions follows the methodology of Stagge and Sung (2022).

Group level smoothers account for model specific seasonal corrections and a model specific intercept. Cyclic spline

215 functions were applied for the seasonal bias term, $f(X_{month}\ by=model)$. Assuming a cyclic function for the recurrent monthly term constrains the model so that late December and early January have similar values, matching up to their second derivative. This term is stationary, i.e., does not change year to year. The $f(X_{month}\ by=model)$ term uses group level smoothers for this seasonal bias spline, so that each dataset applies unique seasonal adjustments to the common tensor product spline. A model-specific intercept, $\beta_{0,model}$ was also included to capture consistent biases between datasets. The variations of smoothing

220 functions and parameter β_s are modeled using 'mgcv' packages in R (Wood, 2008).

Bias correction was conducted based on three assumptions: (1) the GridMET dataset is not systematically biased (Yang et al., 2017), (2) the magnitude of bias can differ by season, and (3) biases are stationary in the long-term, i.e. biases during overlapped periods are representative of biases throughout the rest of the data. Following the first assumption, when plotting results, we adjust CRU and NASPA parameters to match the GridMET dataset. The second and third assumptions are

225 addressed by the $B_{0,Model}+B_1\ f(X_{month,}\ by=model)$ permitting different bias corrections by month and model, which are estimated during overlapping periods and fixed outside this period.
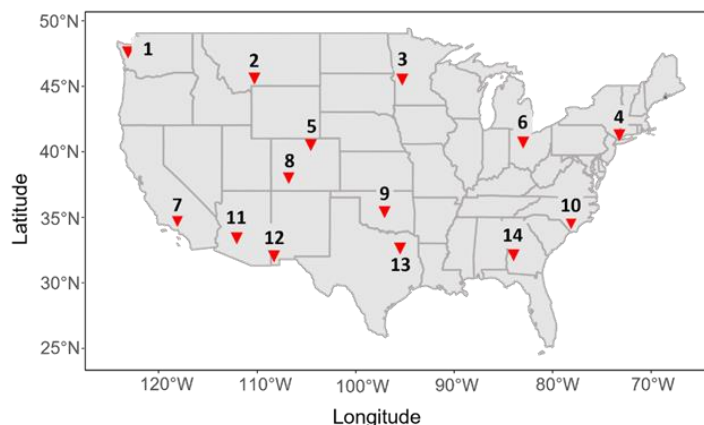
Figure 2. Gauge site locations. The abbreviation of each locations are as follows.1: Aber,WA. 2. Grd,MT. 3. Mor,MN. 4. Nyc,NY. 5. Den,CO. 6. Mrv, OH. 7. Los, CA. 8 Mtn, CO. 9. Okc,OK. 10.Sbw, NC. 11. Phx, AZ. 12. Roe, NM. 13. Wax, TX. 14. Alb, GA

230

The developed model was applied to 14 locations across the continental United States (Figure 2; Table 1). These sites were chosen based on relatively long instrumental records, adequate NASPA reconstruction skill, and to represent a wide range of climate regions. NASPA reconstruction skill, measured by the coefficients of multiple determination (R^2), is shown in Table 1.

235 **Table 1. List of sites considered in this study. The number for each site refers to the location in Fig. 1. NASPA reconstruction skill for the cool (DJFMA) and warm (MJJ) seasons are presented as R2.**

	Symbol	Location	NASPA Skill(R^2)	
			DJFMA	MJJ
1	Aber, WA	Aberdeen, Washington	0.457	0.485
2	Grd, MT	Gardiner, Montana	0.486	0.485
3	Mor, MN	Morrisville, Minnesota	0.347	0.478
4	Nyc, NY	New York City, New York	0.27	0.437
5	Den, CO	Denver, Colorado	0.346	0.671
6	Mrv, OH	Marysville, Ohio	0.295	0.323
7	Los, CA	Los Angeles, California	0.782	0.533
8	Mtv, CO	Monte Vista, Colorado	0.446	0.498
9	Okc, OK	Oklahoma City, Oklahoma	0.441	0.428
10	Sbw, NC	South Brunswick, NC	0.245	0.265
11	Phx, AZ	Phoenix, Arizona	0.58	0.371
12	Roe, NM	Rodeo, New Mexico	0.544	0.366
13	Wax, TX	Waxahachie, Texas	0.365	0.644
14	Alb, GA	Albany, Georgia	0.508	0.220

3 Results

3.1 Temporally downscaled monthly NASPA time series

240 In order to merge the NASPA data with CRU and GridMET, the irregularly spaced NASPA must first be temporally downscaled, or disaggregated, to a regular monthly time step and 3-month duration. The downscaled NASPA (dsNASPA) 3-months averaged time series was constructed at a monthly scale and given the ds- prefix to distinguish it from the original NASPA reconstruction. Figure 3 shows three example years for two sites with very different climatology, showing the ensemble of 10 selected nearest neighbors (pink), the resultant dsNASPA estimate (black), and the true value from the

245 GPCC for those years when data is available (1950 and 2010, blue). Each figure displays 13 months, or one unit of the KNN downscaling process, from the previous year's July to the current July.
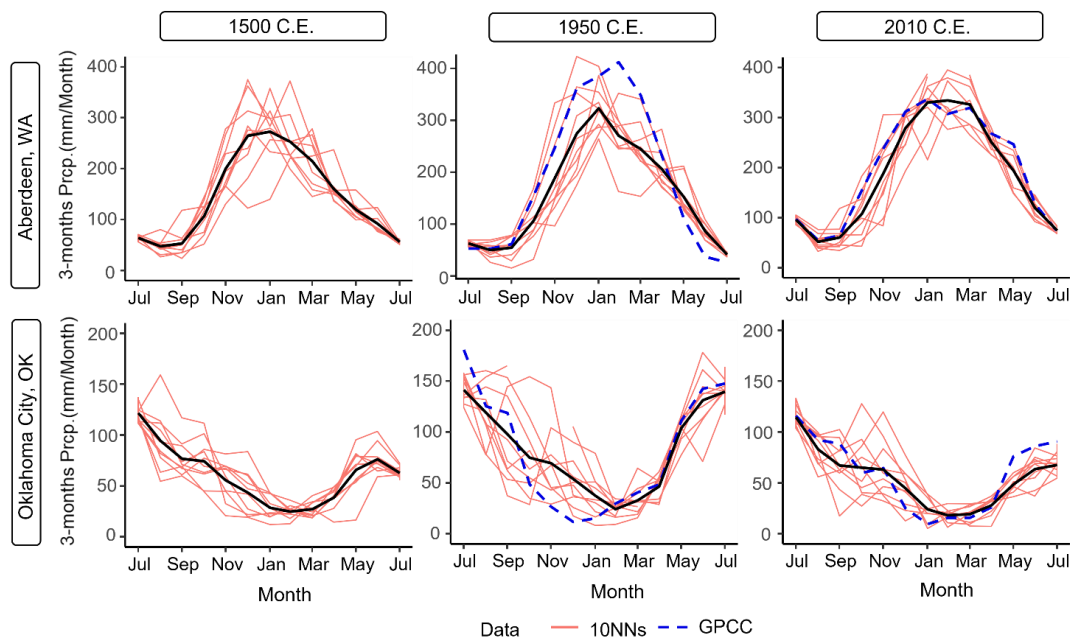
Figure 3.Comparing downscaled NASPA (Black), 10 Nearest Neighbors (pink) and GPCC (blue dashed) at Aberdeen, WA (upper) and Oklahoma City, OK (lower). The marked month in X-axis refers the last month of 3months-rolling average.

250   The dsNASPA generally agrees with the GPCC, especially in capturing seasonality (Fig. 3). Downscaling skill is generally good in the season between DJF-MJJ where the NASPA reconstruction covers all three months (Fig. 3 and Fig.4). July SPI-3 (MJJ) often produces the smallest nMAE, which is logical given that the July SPI-3 period exactly overlaps with the warm season MJJ from the NASPA. Thus, the downscaling process has good information during this period and is not required to do as much.

255   There are a few exceptions showing large nMAE in this period (Figure 4). This occurs in Los, CA, Phx, AZ and Roe, NM which have very low precipitation during the warm season. This large error is related to not capturing occasional large precipitation events using SPI based on the GPCC library and was further exacerbated by extremely small values in the denominator of the nMAE. Despite the limitation, downscaling accurately predicts the general precipitation pattern in terms of seasonal and long-term average precipitation, with nMAE values generally between 0.1 - 0.5. For regions other than the

260   semi-arid locations described above, errors during periods of good NASPA coverage occur primarily due to the errors between sampled GPCC and NASPA. For example, the dry bias shown in July (MJJ) between dsNASPA and GPCC in 1950 at Oklahoma City (Figure 3, center) is caused by uncertainty in the original NASPA dataset, which caused the converged point of nearest neighbors (black) to underestimate precipitation relative to the GPCC observation (blue). May and June (MAM and AMJ, respectively) are reproduced nearly as well, given that these periods share coverage from the cool

265   (DJFMA) and warm (MJJ) reconstructions.

Later periods of the 5-month cool season reconstruction, March (JFM) and April (FMA), show reasonably good accuracy. Error increases through fall and winter as the downscaling approach much interpolate across a temporal gap between

NASPA reconstructions (Fig. 4). This is indicated by much broader resampled estimate ranges (Fig. 3) during the late fall and early winter.
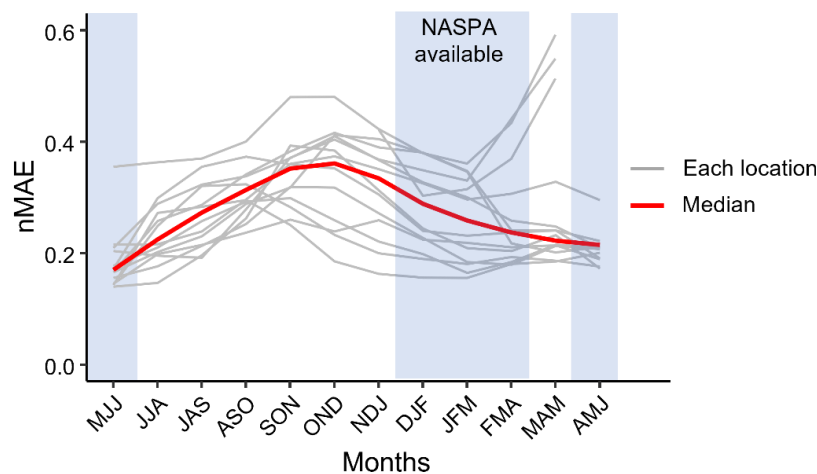
270

Figure 4. nMAE to indicate downscaling skills at each location and its median.

3.2 Investigating Model bias

Here we investigate how dataset bias is quantified in the model. As mentioned, our model accounts for two types of bias: a consistent bias for a given dataset across the entire year and seasonal specific bias. These bias terms were estimated for both

275 the mean and shape parameters.

Typical results for the Monte Vista, CO gauge show how these biases are captured in a single model (Fig. 5). Fig. 5 shows the non-stationary mean estimate for each dataset, represented by colored lines, and the range from SPI = -1.5 to +1.5 as grey shaded regions. Note that the non-stationary mean lines all follow the same trend, simply adjusted up or down based on bias. At this station, NASPA and CRU tend to underestimate precipitation relative to the GridMET benchmark across all four

280 seasons. This consistent offset may be due to the significantly coarser resolution of NASPA and CRU, which may not capture elevation effects, particularly in this mountainous region. The magnitude of bias also differed by season in this example, with the greatest differences visible during the ASO season (Fig. 5). Note that the four periods we highlight in this study were purposefully chosen to mimic NASPA availability, anchored by the MJJ 3-month period, rather than the more commonly used seasons (DJF, MAM, JJA, SON).

285 In addition to bias in the mean parameter, it is possible to detect model bias in the shape parameter, which controls variance, and thus the range between SPI = -1.5 and +1.5. The most notable bias in the shape parameter for the Monte Vista, CO example is for the NASPA, particularly during ASO, where the shape parameter is significantly overestimated, thereby decreasing the variance for the same mean (Fig. 5). This is logical, as the ensemble resampling approach likely decreased extremes for the ASO period where there is no direct NASPA information. The shape parameter bias is negligible for the

290 FMA and MJJ periods, which have full NASPA coverage. Shape parameter bias results for Monte Vista, CO is typical of

other gauges studied here, with largest bias during the interpolated ASO period and little bias in periods with good NASPA information.
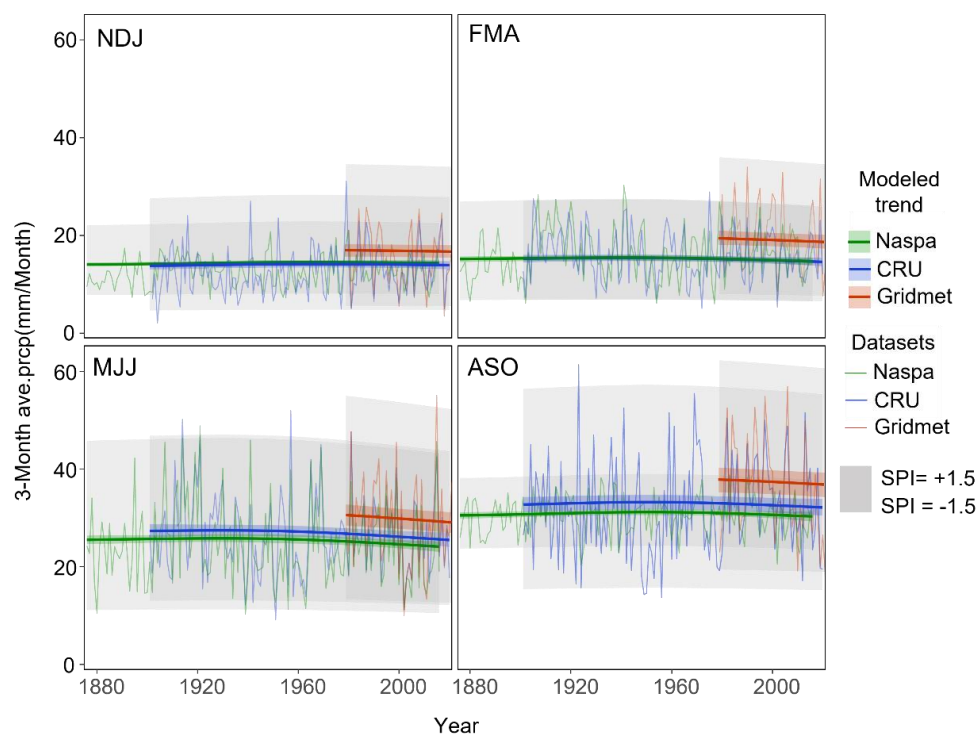
Figure 5. Long-term trends of each dataset for 4 periods at Monte Vista, CO. Mean parameter estimates for each dataset are 295 **represented as differently colored lines, while the SPI -1.5 to 1.5 range for each dataset is indicated by grey regions.**

3.3   Constructing long-term trends

By accounting for the model-induced bias described in Section 3.2 and adjusting all datasets to match GridMET, we were able to generate a 2000-year model of non-stationary precipitation trends for each gauge. The modeled long-term trends incorporating bias correction across all instrumental and proxy datasets in Albany, GA and Monte Vista, CO are presented in 300 Figure 6 as examples to illustrate the results of this approach. Figure 6 represents the long-term mean for each season as a line with a shaded range between SPI of -1.5 and +1.5, similar to Figure 5. The solid black line shows the common, long-term trend of the mean. Fig. 5 focuses on the period 1400 – 2020 year when the original NASPA dataset has the best reconstruction skills (Stahle et al., 2020).

It is noteworthy that all seasons in Albany, GA have experienced abrupt trend changes in recent years, but the direction of 305 change differs by season. Figure 6a shows the warm season (MJJ) has undergone a long-lasting wetting trend from the 1800s to 1900, followed by an abrupt drying trend during the 20th century. Those recent rapid drying trends are manifested in both the mean (SPI = 0) and wet condition (SPI = 1.5). NDJ shows a wetting trend beginning in the mid-1800s and continuing to the present for both wet and dry conditions. The current NDJ mean is the wettest condition of the last 1000 years. This

agrees with previous findings using the NASPA dataset which have identified the southeast US including Albany, GA as
310 experiencing the greatest positive precipitation trend during the DJFMA cool season (Stahle et al., 2020).
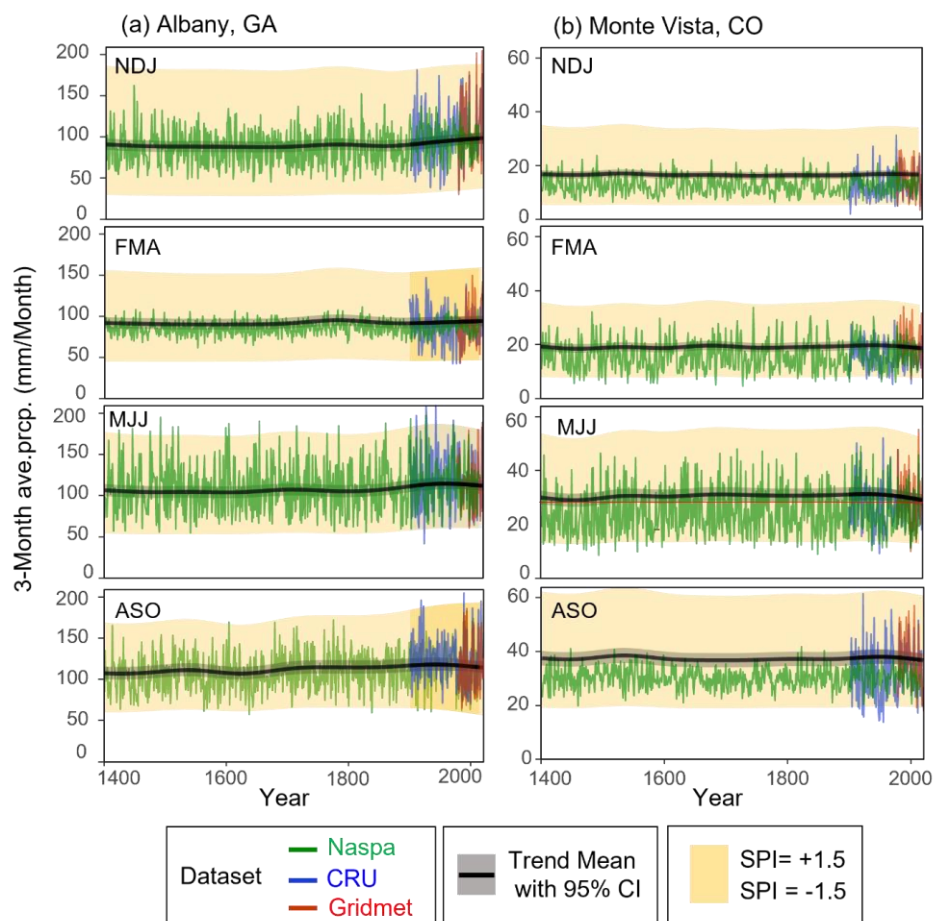
Figure 6. Long-term trends in 3 months NSPI (black line) and averaged precipitations in four periods. The yellow shaded area represents the 95% percentile for the Gamma distribution, so that the upper and lower boundary represents SPI 1.5 and -1.5, respectively. The red line in MJJ highlights the 3 months average precipitation of 2020 as a modern benchmark for comparison.

315 We note that the Albany, GA, site has also experienced changes in the magnitude of variability between dry and wet

extremes. The variance between SPI = 1.5 and SPI = -1.5 during the MJJ season became much larger during the recent

period, particularly for the ASO season, implying both wet and dry conditions have become more extreme in both directions

than during prior centuries. The significant drying trend in MJJ coupled with a wetting trend during the NDJ season indicates

a seasonal shift of the driest season. While NDJ has historically been the driest period among the 4 seasons, during the

320 modern period, MJJ now has similar dry conditions to the NDJ period.

Monte Vista, CO had very stable SPI trends until the 19th century before undergoing a rapid drying trend during the 20th

century, particularly during the MJJ and ASO periods (Fig. 5b). The MJJ mean parameter is currently at its driest value in

approximately 500 years after a long stable period between 1500 and 1900. A red line is shown as a baseline in Fig. 5b to

indicate the modern MJJ mean for comparison against the reconstructed mean. ASO also shows drying trends within the last 300 years.

We can see that the modeled mean of dsNASPA in Monte Vista, CO is shifted upwards from its original average value because of bias correction (Fig. 5b). The dsNASPA contains negative bias which tends to underestimate the drought severity compared to GridMET dataset. Our modeling process detected those biases and calibrated to shift upwards while maintaining a common gradual trend.
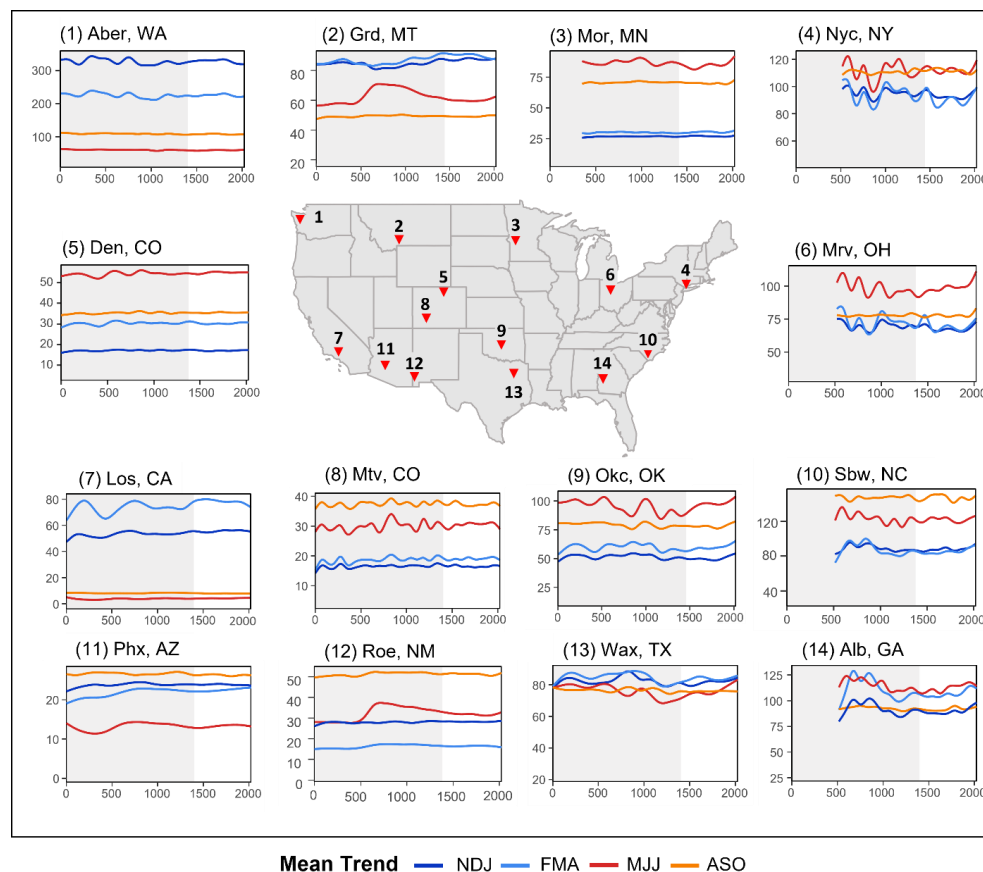
Figure 7. Long-term trends of averaged 3 months precipitation(mm/month) for 4 seasons. The periods before 1400 CE are shaded to represent the period with less prediction skills in original NASPA.

Figure 7 provides long-term trends the four seasons previously discussed across all 14 study sites. The plots show natural seasonality as differences between seasonal lines and long-term climate non-stationarity as changes in each line. This separation allows for an evaluation of recent precipitation trends by comparing the past 100-year trend with the longer 2000 year time window. While results from the entire non-stationary GAM model are presented in Figure 7, extending back to the earliest NASPA reconstructions, our primary focus is on the period after 1400, shown in white. Prior to 1400 CE the NASPA reconstruction has greater uncertainty, and so is provided here for full context, but shaded in grey to emphasize this greater uncertainty. Within the GAM model, this uncertainty manifests as generally less stable estimates.

340   Figure 7 implies a general spatial pattern of recent drying in the western US, and wetting in the eastern US. The drying trend in the west is most prevalent during each sites' wet seasons, with smaller or negligble trends during the driest part of the year. For example, the wet season drying trend is visible in Aber, WA, where after several centuries of stable precipitation there has been a decrease during the cool, wet seasons (NDJ and FMA). The wet season (FMA) in Grd, MT and Los, CA , also show clear drier trends during the most recent century or more. The drier trend in Los, CA, is especially severe: FMA

345   precipitation has declined since 1500 CE but this trend has become more rapid during the 20th century. The 20th century drying trend in Mtv, CO, has occurred across all seasons, not only for the wettest period like the other western stations. The most severe drying trend occurred in MJJ as mentioned in previous section (Fig. 6). The most severe western sites illustrate the value of comparing 20th century drying trends to longer reconstructed records to identify rapid and exceptional precipitation changes. Unlike these western sites, Den, CO, shows negligible long-term trends, while the desert southwest

350   (Phx, AZ and Roe, NM) exhibit minor wetting trends which are largely within the pre-industrial historical range.

The eastern part of the US generally has experienced rapid wetting trends during the most recent century as observed in previous research (Bishop et al., 2021). Those wetting trends are especially drastic in Nyc, NY, Mor, MN, and Mrv, OH, each currently experiencing the wettest conditions of the last 500 years of pre-industial, presumed near natural cyclic variability. This pattern is particularly visible for the warm, wet summer season (MJJ). Sbw, NC also indicates a wetting

355   trend in all seasons since 1700 CE, but those trends are not as rapid as the more northern sites. Warm season (MJJ) precipitaiton has also increased in the southern plains (Okc,OK and Wax,TX). Precipitation during the summer season has been gradually increasing since 1400 CE, but has undergone far more rapid increases since 1900 CE. Note that non-stationarity in the eastern US is less stable, which may be related to greater uncertainty in the NASPA reconstructions for this region with generally poorer reconstruction skill (Table 1, Stahle et al., 2020).

360   Some locations have experienced different direction of changes based on seasons. Those changes mostly occur in southern part of the US as shown in Figure 7 (11 – 14). For example, FMA precipitation in Phx, AZ has become slightly wetter during the last 500 years, while the other three seasons have been slightly drier during the 20th century. Alb, GA shows recent drying trends during the spring and early summer (FMA and MJJ) but wetter trends during fall and winter (ASO and NDJ). Those seasonal specific changes ultimately shift the timing of the wettest or driest season. For example, while the NDJ

365   season has been the driest season during the past 500 years, slightly drier than the preceding ASO season, this has changed during the 20th century. In addition, the difference between the wet seasons (Feb-Jun) and dry seasons (Aug-Jan) is decreasing as the wet seasons become drier and dry seasons become wetter. Seasonal shifts also appeared in Wax, TX, stemming from a constant wetting trend of MJJ season since 1000 CE while other seasons have experienced what is presumed to be natural variability with no abrupt 20th century changes. Though not the focus of this study, our results do

370   capture past drought events such as the prolonged dry period in 1200 -1300s in Okc, OK and Wax, TX, consistent with previous studies regarding the so-called Medieval mega drought (Stahle, 2020; Cook et al., 2016).

4 Discussion

Our novel approach for temporal downscaling, combined bias correction, and non-linear trend modeling enables analyses of
375 meteorological drought changes at a multi-centennial scale. Our downscaling approach allows irregular historical
reconstruction to be included with instrumental records in a single long-term trend model using the same temporal scale, and
ultimately to compare non-stationary drought trends across seasons. The KNN downscaling approach preserves greater
certainty during seasons with NASPA reconstructions and wider uncertainty during seasons that must be interpolated.
Simultaneous temporal trend fitting and bias correction, constrained with a GAM spline model, appears to provide a stable
380 framework to merge these disparate datasets.

In particular, this approach appears successful at generating a continuous sequence of bias-corrected precipitation
distributions while addressing some of nuances of the NASPA reconstruction. The NASPA contains internal bias in
reconstructing precipitation for the cool and warm seasons, with skill varying across the continent. Further, within the cool
or warm period, the reconstruction can be dominated by one or two months. For example, the DJFMA reconstruction in
385 California displays significantly higher correlations with December, January, or February precipitation totals than for March
or April. However, DJFMA was used as a compromise to ensure a common cool period across the US. It appears that
hierarchical GAM bias correction combined with KNN downscaling mitigates some of this effect by creating a local model
for each site. Further, by using a seasonally varying bias correction, the model adjusts to the months, for example within the
DJFMA, that are best captured.

390 We found a general drying trend for the wettest seasons in the western US and wet trends across most seasons in the eastern
US. For some of these sites, 20th century trends appear to be rapid and outside the range of the long-term reconstructed
record, whereas for other sites these patterns could be considered within the pre-industrial range and perhaps part of natural
climate variability. Our results also pointed out some study sites where precipitation trends differ by season, leading to
slightly altered seasonality.

395 Results for the western US agree with previous findings that showed extraordinary drying trends in the western US during
the last century following a prolonged period of stable precipitation patterns since the 1500s (Stahle, 2020) The previously
documented Medieval era megadroughts in the Great Plain region (Cook et al., 2016) also appear in our results. This
consistency of results indicates that incorporating NASPA reconstructions data using our new method is feasible and can be
useful to identify low frequency droughts trends and variability during the past 2000 years.

400 By contrasting the severity of precipitation changes during the past century with 2000 years of data, this model provides a
potential to analyze the magnitude of recent trends during the modern increase in greenhouse gases with pre-Industrial
natural variability. For example, Figures 5, 6b and 7 each present subfigures showing the same meteorological drought trend
model results at Monte Vista, CO. each progressive figure takes a wider temporal viewpoint, from the last 120 years (Fig. 5),
the last 600 years including the pre-Industrial period (Fig. 6b), the longest possible view beginning in 0 CE. As can be seen,
405 the drying trends in Figure 5 are rather steadily decreasing, but do not capture its extraordinary changes shown in Figure 6b.

Taking a longer perspective implies that the modern 120-year data period is outside of the 'pre-industrial levels' defined by UN Paris agreement (IPCC, 2014), with the modern MJJ mean at its driest in 600 years . Our results agree with other findings that have identified recent or projected future shifts in seasonal precipitation (Marvel et al., 2021) or enhanced precipitation variability (Williams et al., 2020) due to anthropogenic climate change. For example, for several western sites, this study observed rapid drying trends during the wettest seasons (Aber, Mtv, Grd, Los). These wet seasons are particularly critical in the western US, which relies on seasonal precipitation to fill reservoirs for later use during dry seasons. We therefore believe that modeling these smooth seasonal shifts over multiple centuries can inform water management plans to adapt to a changing climate. In addition, we believe understanding the seasonal specific changes in meteorological drought can help to analyze seasonal shifts in other types of droughts, such as anticipated summer soil moisture drought southwest US due to declining spring precipitation (Williams et al., 2020).

We expect that our approach described here as a model validation for several case study sites could be applied across a denser network of sites to determine how meteorological drought has changed during the modern instrumental period and to put these trends into a much longer, pre-Industrial context. A unique benefit of this approach is that it models non-linear changes in typical precipitation (SPI=0), droughts (SPI < 0), and pluvials (SPI > 0) simultaneously across all seasons.

5 Conclusion

This study introduced a novel method designed to apply the recently non-stationary SPI approach (Stagge and Sung, 2022) to a multi-century temporal scale by merging disparate datasets with a common tensor product spline term. To accomplish this objective, first we downscaled the irregularly spaced, bi-annual NASPA reconstruction into monthly scale using a KNN approach. This permits analyses at a seasonal scale and enables the NASPA reconstruction to be integrated with instrumental data. We make our data publicly available to allow researchers to access for develop drought trend studies.

Second, we identified unique biases arising from different precipitation data sources and accounted for these biases in a hierarchical GAM model with model-based bias correction. This model corrected both persistent biases and seasonal specific biases. Accounting for unique seasonal biases is important as previous studies have found bias magnitude can vary by season (Piani et al., 2010; Li et al., 2010). This is especially relevant when merging NASPA data, because the temporal downscaling procedure depends strongly on season, e.g., MJJ is made directly from original reconstruction while ASO is based on KNN interpolating between the prior MJJ and the future DJFMA.

Third, after confirming that the temporal downscaling and non-stationary SPI model with bias correction were able to capture long-term trends, this study applied the model to a wide range of case study sites. Analyzing long-term trends in each season permits observation of shifts in seasonality and its variability. Those changes are also captured by season, so that our study could point out a specific season that is experiencing rapid changes although other seasons do not have drastic changes.

References

Abatzoglou, J. T.: Development of gridded surface meteorological data for ecological applications and modelling, Int. J.
440   Climatol., 33, 121–131, https://doi.org/10.1002/joc.3413, 2013.

Ault, T. R.: On the essentials of drought in a changing climate, Science, 368, 256–260, https://doi.org/10.1126/science.aaz5492, 2020.

Baek, S. H., Smerdon, J. E., Coats, S., Williams, A. P., Cook, B. I., Cook, E. R., and Seager, R.: Precipitation, Temperature,
445   and Teleconnection Signals across the Combined North American, Monsoon Asia, and Old World Drought Atlases, J. Clim.,
30, 7141–7155, https://doi.org/10.1175/JCLI-D-16-0766.1, 2017.

Becker, A., Finger, P., Meyer-Christoffer, A., Rudolf, B., Schamm, K., Schneider, U., and Ziese, M.: A description of the
global land-surface precipitation data products of the Global Precipitation Climatology Centre with sample applications
450   including centennial (trend) analysis from 1901–present, Earth Syst. Sci. Data, 5, 71–99, https://doi.org/10.5194/essd-5-71-
2013, 2013.

Bishop, D. A., Williams, A. P., Seager, R., Cook, E. R., Peteet, D. M., Cook, B. I., Rao, M. P., and Stahle, D. W.: Placing
the east-west North American aridity gradient in a multi-century context, Environ. Res. Lett., 16, 114043,
455   https://doi.org/10.1088/1748-9326/ac2f63, 2021.

Coats, S., Smerdon, J. E., Seager, R., Griffin, D., and Cook, B. I.: Winter-to-summer precipitation phasing in southwestern
North America: A multicentury perspective from paleoclimatic model-data comparisons, J. Geophys. Res. Atmospheres,
120, 8052–8064, https://doi.org/10.1002/2015JD023085, 2015.
460

Cook, B. I., Ault, T. R., and Smerdon, J. E.: Unprecedented 21st century drought risk in the American Southwest and Central
Plains, Sci. Adv., 1, e1400082, https://doi.org/10.1126/sciadv.1400082, 2015.

Cook, B. I., Cook, E. R., Smerdon, J. E., Seager, R., Williams, A. P., Coats, S., Stahle, D. W., and Díaz, J. V.: North
465   American megadroughts in the Common Era: reconstructions and simulations, WIREs Clim. Change, 7, 411–432,
https://doi.org/10.1002/wcc.394, 2016.

Cook, E. R. and Krusic, P. J.: North American Summer PDSI Reconstructions, Version 2a, NOAA/NGDC Paleoclimatology
Program, Boulder CO, USA, 2008.

470 Cook, E. R., Meko, D. M., Stahle, D. W., and Cleaveland, M. K.: Drought Reconstructions for the Continental United States, J. Clim., 12, 1145–1162, https://doi.org/10.1175/1520-0442(1999)012<1145:DRFTCU>2.0.CO;2, 1999.

Cook, E. R., Anchukaitis, K. J., Buckley, B. M., D'Arrigo, R. D., Jacoby, G. C., and Wright, W. E.: Asian Monsoon Failure and Megadrought During the Last Millennium, Science, 328, 486–489, https://doi.org/10.1126/science.1185188, 2010a.

475

Cook, E. R., Seager, R., Heim, R. R., Vose, R. S., Herweijer, C., and Woodhouse, C.: Megadroughts in North America: placing IPCC projections of hydroclimatic change in a long-term palaeoclimate context, J. Quat. Sci., 25, 48–61, https://doi.org/10.1002/jqs.1303, 2010b.

480 Dai, A.: Drought under global warming: a review, WIREs Clim. Change, 2, 45–65, https://doi.org/10.1002/wcc.81, 2011.
Diffenbaugh, N. S., Swain, D. L., and Touma, D.: Anthropogenic warming has increased drought risk in California, Proc. Natl. Acad. Sci., 112, 3931–3936, https://doi.org/10.1073/pnas.1422385112, 2015.

Easterling, D. R., Evans, J. L., Groisman, P. Y., Karl, T. R., Kunkel, K. E., and Ambenje, P.: Observed Variability and
485 Trends in Extreme Climate Events: A Brief Review, Bull. Am. Meteorol. Soc., 81, 417–426, https://doi.org/10.1175/1520-0477(2000)081<0417:OVATIE>2.3.CO;2, 2000.

Franke, J., Frank, D., Raible, C. C., Esper, J., and Brönnimann, S.: Spectral biases in tree-ring climate proxies, Nat. Clim. Change, 3, 360–364, https://doi.org/10.1038/nclimate1816, 2013.

490

Gangopadhyay, S., Clark, M., and Rajagopalan, B.: Statistical downscaling using K-nearest neighbors, Water Resour. Res., 41, https://doi.org/10.1029/2004WR003444, 2005.

Gangopadhyay, S., Harding, B. L., Rajagopalan, B., Lukas, J. J., and Fulp, T. J.: A nonparametric approach for
495 paleohydrologic reconstruction of annual streamflow ensembles, Water Resour. Res., 45, https://doi.org/10.1029/2008WR007201, 2009.

Gutmann, E. D., Rasmussen, R. M., Liu, C., Ikeda, K., Gochis, D. J., Clark, M. P., Dudhia, J., and Thompson, G.: A Comparison of Statistical and Dynamical Downscaling of Winter Precipitation over Complex Terrain, J. Clim., 25, 262–281,
500 https://doi.org/10.1175/2011JCLI4109.1, 2012.

Guttman, N. B.: Accepting the Standardized Precipitation Index: A Calculation Algorithm1, JAWRA J. Am. Water Resour. Assoc., 35, 311–322, https://doi.org/10.1111/j.1752-1688.1999.tb03592.x, 1999.

Harris, I., Osborn, T. J., Jones, P., and Lister, D.: Version 4 of the CRU TS monthly high-resolution gridded multivariate
505   climate dataset, Sci. Data, 7, 109, https://doi.org/10.1038/s41597-020-0453-3, 2020.

Herweijer, C., Seager, R., Cook, E. R., and Emile-Geay, J.: North American Droughts of the Last Millennium from a
Gridded Network of Tree-Ring Data, J. Clim., 20, 1353–1376, https://doi.org/10.1175/JCLI4042.1, 2007.

510   Ho, C. K., Stephenson, D. B., Collins, M., Ferro, C. A. T., and Brown, S. J.: Calibration Strategies: A Source of Additional
Uncertainty in Climate Change Projections, Bull. Am. Meteorol. Soc., 93, 21–26, https://doi.org/10.1175/2011BAMS3110.1,
2012.

Howard, I. M., Stahle, D. W., Torbenson, M. C. A., and Griffin, D.: The summer precipitation response of latewood tree-ring
515   chronologies in the southwestern United States, Int. J. Climatol., 41, 2913–2933, https://doi.org/10.1002/joc.6997, 2021.
IPCC: Climate Change 2013: The Physical Science Basis: Working Group I Contribution to the Fifth Assessment Report of
the Intergovernmental Panel on Climate Change, Cambridge University Press, 1553 pp., 2014.

Konapala, G., Mishra, A. K., Wada, Y., and Mann, M. E.: Climate change will affect global water availability through
520   compounding changes in seasonal precipitation and evaporation, Nat. Commun., 11, 3044, https://doi.org/10.1038/s41467-
020-16757-w, 2020.

Lanzante, J. R., Dixon, K. W., Nath, M. J., Whitlock, C. E., and Adams-Smith, D.: Some Pitfalls in Statistical Downscaling
of Future Climate, Bull. Am. Meteorol. Soc., 99, 791–803, https://doi.org/10.1175/BAMS-D-17-0046.1, 2018.
525

Li, H., Sheffield, J., and Wood, E. F.: Bias correction of monthly precipitation and temperature fields from
Intergovernmental Panel on Climate Change AR4 models using equidistant quantile matching, J. Geophys. Res.
Atmospheres, 115, https://doi.org/10.1029/2009JD012882, 2010.

530   Lloyd-Hughes, B. and Saunders, M. A.: A drought climatology for Europe, Int. J. Climatol., 22, 1571–1592,
https://doi.org/10.1002/joc.846, 2002.

Marvel, K., Cook, B. I., Bonfils, C. J. W., Durack, P. J., Smerdon, J. E., and Williams, A. P.: Twentieth-century
hydroclimate changes consistent with human influence, Nature, 569, 59–65, https://doi.org/10.1038/s41586-019-1149-8,
535   2019.

Marvel, K., Cook, B. I., Bonfils, C., Smerdon, J. E., Williams, A. P., and Liu, H.: Projected Changes to Hydroclimate Seasonality in the Continental United States, Earths Future, 9, e2021EF002019, https://doi.org/10.1029/2021EF002019, 2021.

540   Maurer, E. P., Wood, A. W., Adam, J. C., Lettenmaier, D. P., and Nijssen, B.: A Long-Term Hydrologically Based Dataset of Land Surface Fluxes and States for the Conterminous United States, J. Clim., 15, 3237–3251, https://doi.org/10.1175/1520-0442(2002)015<3237:ALTHBD>2.0.CO;2, 2002.

Mishra, V., Cherkauer, K. A., and Shukla, S.: Assessment of Drought due to Historic Climate Variability and Projected
545   Future Climate Change in the Midwestern United States, J. Hydrometeorol., 11, 46–68, https://doi.org/10.1175/2009JHM1156.1, 2010.

New, M., Hulme, M., and Jones, P.: Representing Twentieth-Century Space–Time Climate Variability. Part II: Development of 1901–96 Monthly Grids of Terrestrial Surface Climate, J. Clim., 13, 2217–2238, https://doi.org/10.1175/1520-
550   0442(2000)013<2217:RTCSTC>2.0.CO;2, 2000.

Pal, I., Anderson, B. T., Salvucci, G. D., and Gianotti, D. J.: Shifting seasonality and increasing frequency of precipitation in wet and dry seasons across the U.S., Geophys. Res. Lett., 40, 4030–4035, https://doi.org/10.1002/grl.50760, 2013.

555   Palmer, W. C.: Meteorological Drought, U.S. Department of Commerce, Weather Bureau, 68 pp., 1965.

Patel, N. R., Chopra, P., and Dadhwal, V. K.: Analyzing spatial patterns of meteorological drought using standardized precipitation index, Meteorol. Appl., 14, 329–336, https://doi.org/10.1002/met.33, 2007.

560   Pedersen, E. J., Miller, D. L., Simpson, G. L., and Ross, N.: Hierarchical generalized additive models in ecology: an introduction with mgcv, PeerJ, 7, e6876, https://doi.org/10.7717/peerj.6876, 2019.

Piani, C., Weedon, G. P., Best, M., Gomes, S. M., Viterbo, P., Hagemann, S., and Haerter, J. O.: Statistical bias correction of global simulated daily precipitation and temperature for the application of hydrological models, J. Hydrol., 395, 199–215,
565   https://doi.org/10.1016/j.jhydrol.2010.10.024, 2010.

Pollock, M. D., O'Donnell, G., Quinn, P., Dutton, M., Black, A., Wilkinson, M. E., Colli, M., Stagnaro, M., Lanza, L. G., Lewis, E., Kilsby, C. G., and O'Connell, P. E.: Quantifying and Mitigating Wind-Induced Undercatch in Rainfall Measurements, Water Resour. Res., 54, 3863–3875, https://doi.org/10.1029/2017WR022421, 2018.

570 Raje, D. and Mujumdar, P. P.: A comparison of three methods for downscaling daily precipitation in the Punjab region, Hydrol. Process., 25, 3575–3589, https://doi.org/10.1002/hyp.8083, 2011.

Robeson, S. M., Maxwell, J. T., and Ficklin, D. L.: Bias Correction of Paleoclimatic Reconstructions: A New Look at 1,200+ Years of Upper Colorado River Flow, Geophys. Res. Lett., 47, e2019GL086689, 575 https://doi.org/10.1029/2019GL086689, 2020.

Schubert, S. D., Stewart, R. E., Wang, H., Barlow, M., Berbery, E. H., Cai, W., Hoerling, M. P., Kanikicharla, K. K., Koster, R. D., Lyon, B., Mariotti, A., Mechoso, C. R., Müller, O. V., Rodriguez-Fonseca, B., Seager, R., Seneviratne, S. I., Zhang, L., and Zhou, T.: Global Meteorological Drought: A Synthesis of Current Understanding with a Focus on SST Drivers of 580 Precipitation Deficits, J. Clim., 29, 3989–4019, https://doi.org/10.1175/JCLI-D-15-0452.1, 2016.

Shiau, J.-T.: Effects of Gamma-Distribution Variations on SPI-Based Stationary and Nonstationary Drought Analyses, Water Resour. Manag., 34, 2081–2095, https://doi.org/10.1007/s11269-020-02548-x, 2020.

585 Simpson, G. L.: Modelling Palaeoecological Time Series Using Generalised Additive Models, Front. Ecol. Evol., 6, https://doi.org/10.3389/fevo.2018.00149, 2018.

St. George, S., Meko, D. M., and Cook, E. R.: The seasonality of precipitation signals embedded within the North American Drought Atlas, The Holocene, 20, 983–988, https://doi.org/10.1177/0959683610365937, 2010.
590
Stagge, J. H. and Sung, K.: A Non-stationary Standardized Precipitation Index (NSPI) using Bayesian Splines, J. Appl. Meteorol. Climatol., 1, https://doi.org/10.1175/JAMC-D-21-0244.1, 2022.

Stagge, J. H., Tallaksen, L. M., Gudmundsson, L., Loon, A. F. V., and Stahl, K.: Candidate Distributions for Climatological 595 Drought Indices (SPI and SPEI), Int. J. Climatol., 35, 4027–4040, https://doi.org/10.1002/joc.4267, 2015.

Stagge, J. H., Kingston, D. G., Tallaksen, L. M., and Hannah, D. M.: Observed drought indices show increasing divergence across Europe, Sci. Rep., 7, 1–10, https://doi.org/10.1038/s41598-017-14283-2, 2017.

600 Stahle, D. W.: Anthropogenic megadrought, Science, 368, 238–239, https://doi.org/10.1126/science.abb6902, 2020.

Stahle, D. W., Cook, E. R., Burnette, D. J., Torbenson, M. C. A., Howard, I. M., Griffin, D., Diaz, J. V., Cook, B. I., Williams, A. P., Watson, E., Sauchyn, D. J., Pederson, N., Woodhouse, C. A., Pederson, G. T., Meko, D., Coulthard, B., and

Crawford, C. J.: Dynamics, Variability, and Change in Seasonal Precipitation Reconstructions for North America, J. Clim., 33, 3173–3195, https://doi.org/10.1175/JCLI-D-19-0270.1, 2020.

Sun, Q., Miao, C., Duan, Q., Ashouri, H., Sorooshian, S., and Hsu, K.-L.: A Review of Global Precipitation Data Sets: Data Sources, Estimation, and Intercomparisons, Rev. Geophys., 56, 79–107, https://doi.org/10.1002/2017RG000574, 2018.

Sung, K. and Stagge, J. H.: Non-linear seasonal and long-term trends in a 20th century meteorological drought index across the continental US, J. Clim., 1, 1–31, https://doi.org/10.1175/JCLI-D-22-0045.1, 2022.

Svoboda, M., LeComte, D., Hayes, M., Heim, R., Gleason, K., Angel, J., Rippey, B., Tinker, R., Palecki, M., Stooksbury, D., Miskus, D., and Stephens, S.: THE DROUGHT MONITOR, Bull. Am. Meteorol. Soc., 83, 1181–1190, https://doi.org/10.1175/1520-0477-83.8.1181, 2002.

Torbenson, M. C. A. and Stahle, D. W.: The Relationship between Cool and Warm Season Moisture over the Central United States, 1685–2015, J. Clim., 31, 7909–7924, https://doi.org/10.1175/JCLI-D-17-0593.1, 2018.

Torbenson, M. C. A., Stahle, D. W., Howard, I. M., Burnette, D. J., Griffin, D., Villanueva-Díaz, J., and Cook, B. I.: Drought Relief and Reversal over North America from 1500 to 2016, Earth Interact., 25, 94–107, https://doi.org/10.1175/EI-D-20-0020.1, 2021.

Trenberth, K.: Changes in precipitation with climate change, Clim. Res., 47, 123–138, https://doi.org/10.3354/cr00953, 2011.

Trenberth, K. E., Dai, A., van der Schrier, G., Jones, P. D., Barichivich, J., Briffa, K. R., and Sheffield, J.: Global warming and changes in drought, Nat. Clim. Change, 4, 17–22, https://doi.org/10.1038/nclimate2067, 2014.

Ukkola, A. M., Kauwe, M. G. D., Roderick, M. L., Abramowitz, G., and Pitman, A. J.: Robust Future Changes in Meteorological Drought in CMIP6 Projections Despite Uncertainty in Precipitation, Geophys. Res. Lett., 47, e2020GL087820, https://doi.org/10.1029/2020GL087820, 2020.

Van Loon, A. F., Stahl, K., Di Baldassarre, G., Clark, J., Rangecroft, S., Wanders, N., Gleeson, T., Van Dijk, A. I. J. M., Tallaksen, L. M., Hannaford, J., Uijlenhoet, R., Teuling, A. J., Hannah, D. M., Sheffield, J., Svoboda, M., Verbeiren, B., Wagener, T., and Van Lanen, H. A. J.: Drought in a human-modified world: reframing drought definitions, understanding, and analysis approaches, Hydrol. Earth Syst. Sci., 20, 3631–3650, https://doi.org/10.5194/hess-20-3631-2016, 2016.

Weiss, J. L., Castro, C. L., and Overpeck, J. T.: Distinguishing Pronounced Droughts in the Southwestern United States:

640   Seasonality and Effects of Warmer Temperatures, J. Clim., 22, 5918–5932, https://doi.org/10.1175/2009JCLI2905.1, 2009.

Williams, A. P., Cook, E. R., Smerdon, J. E., Cook, B. I., Abatzoglou, J. T., Bolles, K., Baek, S. H., Badger, A. M., and Livneh, B.: Large contribution from anthropogenic warming to an emerging North American megadrought, Science, 368, 314–318, https://doi.org/10.1126/science.aaz9600, 2020.

645

Wood, S. N.: Fast stable direct fitting and smoothness selection for generalized additive models, J. R. Stat. Soc. Ser. B Stat. Methodol., 70, 495–518, https://doi.org/10.1111/j.1467-9868.2007.00646.x, 2008.

Yang, Z., Hsu, K., Sorooshian, S., Xu, X., Braithwaite, D., Zhang, Y., and Verbist, K. M. J.: Merging high-resolution

650   satellite-based precipitation fields and point-scale rain gauge measurements—A case study in Chile, J. Geophys. Res. Atmospheres, 122, 5267–5284, https://doi.org/10.1002/2016JD026177, 2017.